Modeling the structure and electronic properties of TiO_2 nanoparticles

A. S. Barnard,[1] S. Erdin,[2,3] Y. Lin,[2] P. Zapol,[1,4,*] and J. W. Halley[2]
[1]*Center for Nanoscale Materials, Argonne National Laboratory, 9700 South Cass Avenue, Argonne, Illinois 60439, USA*
[2]*School of Physics and Astronomy, University of Minnesota, Minneapolis, Minnesota 55455, USA*
[3]*Advanced Photon Source, Argonne National Laboratory, 9700 South Cass Avenue, Argonne, Illinois 60439, USA*
[4]*Materials Science and Chemistry Divisions, Argonne National Laboratory, 9700 South Cass Avenue, Argonne, Illinois 60439, USA*
(Received 21 June 2005; revised manuscript received 14 September 2005; published 9 May 2006)

A self-consistent tight-binding method and density functional theory were used to study structures and electronic properties of anatase nanoparticles. Full geometry optimization resulted in both surface relaxation and a slight overall contraction of the nanoparticles. Analyzing electronic properties using electron localization function and Mulliken populations, we found nonbonding electrons at the edges and corners of the nanoparticle. The results of tight-binding and density functional theory calculations are in good agreement, suggesting the tight-binding scheme to be a useful tool for studies of larger nanoparticles in the range of hundreds to thousands of atoms. The self-consistent tight-binding results on nanoparticles of sizes up to 1365 atoms and some structural, electronic, and energetic trends as a function of nanoparticle size are also reported.

DOI: 10.1103/PhysRevB.73.205405 PACS number(s): 61.46.−w, 64.70.Nd, 68.35.−p, 78.67.Bf

I. INTRODUCTION

Titania (TiO_2) nanoparticles are of interest for a variety of technical applications including advanced photochemistry and bioprobes.[1,2] Of the three commonly observed crystal structures of TiO_2, two, anatase and rutile, are energetically very close to one another, which may lead to transitions from one form to the other as function of temperature and crystallite size. Though extensive work has been reported on the electronic and atomic structure of bulk anatase and rutile, as well as some studies of their low index surfaces,[3] less is known about the electronic and atomic structure of nanocrystals of these materials. Recently, a study of spherical TiO_2 nanoparticles using classical interatomic potentials has been reported.[4] Electronic structure calculations of nanoparticles are challenging because experimentally relevant nanoparticles often lie in a size range above the upper limit of feasible first principles electronic structure calculations (10^3–10^4 atoms). To approach this problem, one can use a thermodynamic approach that uses surface, edge and vertex energies, calculated from first principles or determined experimentally, in order to make predictions about the shapes and energetics of large crystallites, using surface and edge energies.[5–8] Such an approach may be valid for large crystallites but it will become less reliable as the crystallites size decreases. In intermediate size ranges one can use self-consistent empirical methods fitted to first-principles calculations on smaller clusters or bulk material to interpolate between the first-principles results and the regime in which the thermodynamic models based on parameters from the periodic calculations are valid.

Here, we describe results of a study of anatase nanoparticles in which we have made first principles calculations on a small nanoparticle (105 atoms) and also self-consistent tight-binding (SCTB) calculations on the same particle in addition to a number of larger examples, up to 1365 atoms in size. We demonstrate that the SCTB method is in reasonable agreement with the density functional theory (DFT) for the small crystallite, validating the use of the SCTB results in determining how the electronic and atomic structure evolves as the crystallite size increases.

II. FIRST PRINCIPLES METHODOLOGY

The first principles calculations have been carried out using DFT within the generalized gradient approximation (GGA), with the exchange-correlation functional of Perdew and Wang (PW91).[9] This has been implemented via the Vienna *Ab initio* Simulation Package,[10,11] which spans reciprocal space with a plane-wave basis up, in this case, to a kinetic energy cutoff of 269.95 eV. We have used the linear tetrahedron method for Brillouin zone integration, and a relaxation technique involving an efficient matrix-diagonalization routine based on a sequential band-by-band residual minimization method of single-electron energies,[12,13] with direct inversion in the iterative subspace.

During the relaxations we have used ultrasoft (US), gradient-corrected Vanderbilt-type pseudopotentials[14,15] and real-space projected wave functions (to decrease the computational cost), and have relaxed to a convergence of 10^{-4} eV. The following (final) calculations of the electron charge density (ECD) and the electron localization function (ELF) were then performed using the projected augmented wave (PAW) potentials,[16] with a basis set increased by 30% and reciprocal-space projected wave functions (to improve accuracy), also to a convergence of 10^{-4} eV. PAW potentials are generally considered to be more accurate than the ultrasoft pseudopotentials,[17] since the radial cutoffs (core radii) are smaller than the radii used for the US pseudopotentials, and the fact that the PAW potentials reconstruct the exact valence wave function with all nodes in the core region.

III. SELF-CONSISTENT TIGHT-BINDING METHODS

Details of the SCTB method have been quite fully described elsewhere.[18–20] The formal description is based on

the Kohn-Sham variational principle,[21] which we formulate in a tight-binding context. We select a small, physically reasonable tight-binding basis for each element. Through minimization of an energy functional, we obtain effective one-electron equations which are solved self-consistently in the Mulliken charges at each atomic site. Correlations are implicitly included in onsite energies, which are functions of the local charges and, in some cases, of the ionic spins. These onsite functions, which describe the model in the limit of infinite separation of the atoms, are fitted as a function of ionic charge and spin to the known ionic energy levels. The remaining parameters of the tight-binding model fix intersite matrix elements of the kinetic energy, contributions to electrostatic multipoles at each site (subject to constraints of the Wigner-Eckhart theorem) and onsite "environmental" terms associated with each atomic site. The latter account for the effects of atomic neighbors on the onsite matrix elements associated with orbitals assigned to each site. These remaining parameters are fitted by requiring that the self-consistent tight-binding model reproduces the cohesive energies and band structures of a selected set of distorted periodic bulk solid structures, as calculated from a first principles method [here DFT implemented in local density approximation (LDA) in a plane wave basis].[22] The number of parameters for an oxide is of the order of 50.

The SCTB parametrization used in the present calculations is significantly different from that which was reported in the previous work.[18,19] The parametrization used here and summarized in the Appendix is consistent with that used for Ti-Ti interactions in our recently reported SCTB simulations of titanium metal surfaces[20] and with the parametrization of O-O interactions in our recent SCTB model of dissociable water.[23] The Ti-O parameters used here and reported in the Appendix were obtained by fitting first principles data on bulk rutile (essentially the same first principles data base used in Refs. 18 and 19) under the constraint that the Ti-Ti and O-O parameters were fixed as reported in Refs. 20 and 23. Fitting methods were described in Ref. 18. Note that in the present SCTB model, there are nine basis states associated with each Ti ion (5 *d*, 3 *p*, and 1 *s*) consistent with Ref. 20, whereas in the model of Refs. 18 and 19 there were just five *d* states associated with each Ti. These extra states were included for consistency with the model for the metal because we later plan to study metal oxide interfaces using this model. They are unlikely to significantly affect the properties of the bulk oxides because they lie far above the Fermi level. Although the first principles data base used in the fit did not include any information about bulk anatase structure, the anatase structure is well reproduced by this set of parameters (a=3.78 Å and c=9.7 Å). The calculated SCTB cohesive energy for bulk anatase in this parametrization was very slightly above that found for rutile with the same parametrization, consistent with experiment and with some first principles calculations. Calculated Kohn-Sham orbital densities of states from the SCTB model for bulk anatase showed a gap between the valence and conduction bands, correctly predicting that bulk anatase is an insulator. We also report the SCTB surface energies for low index anatase surfaces in Table I, where semi-infinite surfaces were approximated by slabs in the calculations. These energies lie in between LDA and GGA results, which are given for comparison. Thus, the quality of the results is comparable to first principles calculations.

TABLE I. Surface energies (J/m^2) calculated using SCTB and their comparison to DFT results. LDA results are from Ref. 31, PBE results are from Ref. 31, PW91 results are from Ref. 27.

Surface	SCTB	LDA	PBE	PW91
(001)	1.25	1.38	0.9	0.51
(100)	0.67	0.96	0.53	0.39
(101)	0.54	0.84	0.44	0.35

IV. *AB INITIO* RESULTS

The low-energy electronic structure of a 105 atom bipyramidal anatase nanoparticle has been investigated by relaxing the structure and then characterizing the bonding via examination of the ECD and ELF in three dimensions. The stoichiometric nanocrystal with an apex-to-apex length of 22.96 Å was generated using a Wulff[24] construction based on

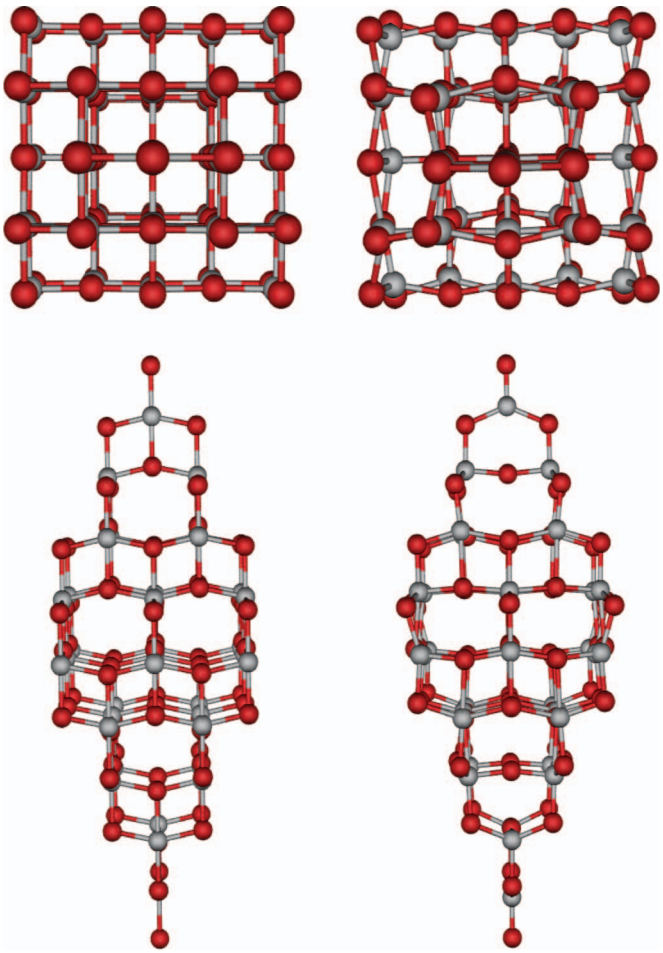

FIG. 1. (Color) The anatase bipyramidal nanocrystal before (left) and after (right) the relaxation, viewed from the [001] direction (top) and [100] direction (bottom).

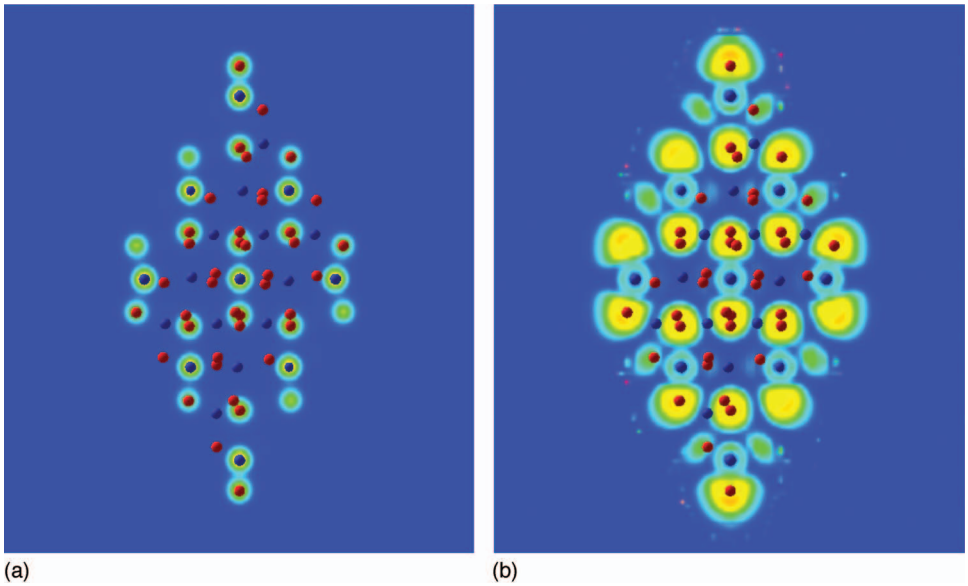

FIG. 2. (Color) (a) The ECD through the central plane of the final relaxed anatase nanoparticle. The localization of the ECD around the Ti (blue) and O (red) atoms indicates a high ionic character. (b) The ELF through the central plane of the final relaxed anatase nanoparticle. The colored plumes of the ELF indicate the presence of nonbonding electrons.

{101} surfaces only, and surrounded by a 15 Å vacuum layer in all directions to create an isolated particle. A Wulff construction including the {001} surfaces would have {001} facets at the apices of this nanocrystal, yielding a truncated bipyramid. We report SCTB results on truncated bipyramids in the next section. The nanoparticle initially consisted of a {101} bulk-terminated (1×1) surface structure, with both Ti and O under-coordinated surface sites.

The final relaxed structure of the nanocrystal may be characterized in a number of ways, including (but not limited to) examination of the atomic displacements via the radial distribution function $G(r)$, the surface structure, the ECD, the ELF and full-crystal relaxations (such as the volume dilation resulting from the reduction of the surface stress during the relaxation procedure). These aspects have been listed below, in comparison with bulk anatase. Figure 1 shows various views of the initial (left) and final relaxed (right) nanocrystal.

A. Relaxed structure

Using the *ab initio* technique outlined above, the energy per TiO_2 unit E_{rel} associated with the relaxation of the nanoparticle was found to be −0.772 eV/atom, and the changes in the structure induced by this energy minimization are as follows. The apex-to-apex length reduced from 22.96 to 22.82 Å, and the bipyramidal side length reduced from 7.56 to 7.47 Å. While this does not seem large, it does produce a volume dilation due to the surface (edge and corner) stress of −3.1%, which is of similar magnitude to the contraction observed previously with other nanocrystals in this size range.[25] This contraction was not limited to the inward relaxation of the surface trilayer, but involved a contraction of the bond lengths even in the center of the nanoparticle, and may therefore be considered as a "full-crystal" relaxation. For example, following the relaxation, a central Ti atom was found to have two (long) apical and four (short)

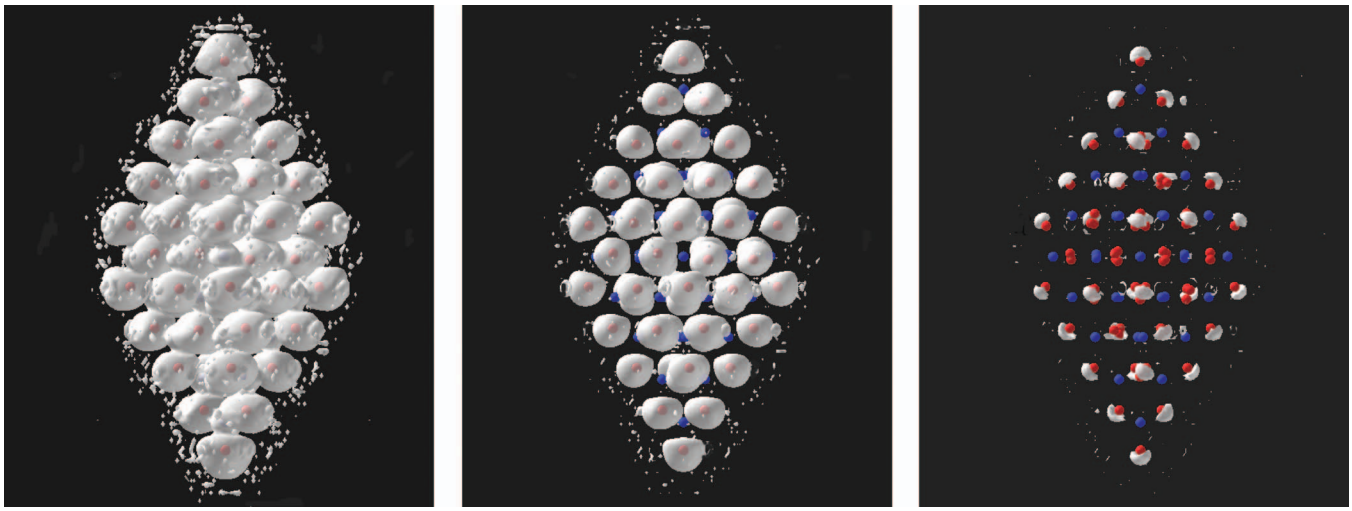

FIG. 3. (Color) Iso-surface applied at $l(r)=0.2$ (left), $l(r)=0.5$ (center) and $l(r)=0.8$ (right) of the ELF for the relaxed 105 atom anatase nanoparticle.

TABLE II. Nanoparticle energies (eV) with respect to bulk calculated using SCTB (DFT value in parentheses). ΔE is given by the particle energy per formula unit less the bulk energy per formula unit. Apex-to-apex and side length distances are given in Å.

Atoms in particle	ΔE	Apex	Side
99	1.44	19.61	7.53
105	1.41 (1.03)	24.86 (22.82)	7.53 (7.47)
417	0.89	23.08	15.15
453	0.844	27.26	15.20
495	0.836	42.19	15.22
1365	0.56	60.93	22.74

equatorial bond lengths of 1.94 and 1.91 Å, respectively. This is considerably less than the bulk experimental values of 1.976 and 1.946 Å, respectively (at 15 K).[26]

The changes in the surface structure of the nanoparticle were dominated by the outward relaxation of the O atoms, and the inward relaxation of the Ti atoms. This created a more rippled or puckered effect on the surface (see Fig. 1), and is consistent with the trend observed in bulk-anatase surfaces.[27] The exception to this trend are the four atoms located at each apex (one Ti and three O), where all atoms contract inwards. Although the apical bonds of the terminal O atoms at the apex contracted to 1.63 Å, the inward relaxation of the O atoms in the next [001] atomic layer caused the bond angle of the apex atoms to increase from 101.8° to 112.4°. It is also interesting to note that the apical O atoms opposing the terminal apex atoms have relaxed inward to the extent that the distance to the Ti atom has increased from 1.98 to 2.68 Å at both apices. These atoms therefore reduce coordination upon relaxation, as supported by examination of the ECD in the next section.

B. Electronic properties

A two-dimensional ECD profile through the central plane of the relaxed anatase nanocrystal was of little help in isolating the bonds present in the structure. As shown in Fig. 2(a), the ECD associated with the Ti (blue) and O (red) atoms is localized around the atom, rather than between the atoms (in the region typically associated with a bond). (The regions of high ECD are colored red and low ECD are colored blue.) This is typical for an ionic material, or bonding with a high ionic character. The ECD does not however, give any information as to the presence of any dangling surface bonds.

Another way to analyze the electronic structure of a material such as a nanocrystal is to use the electron localization function (ELF). To motivate the ELF, Becke and Edgecombe[28] consider the Hartree-Fock probability $P(r_1, r_2|r_1)$ that, given an electron at $\vec{r}_1$ with a given spin, there is another electron at $\vec{r}_2$ with the same spin. Expanding $P(r_1, r_2|r_1)$ as a Taylor series in $s=|\vec{r}_1-\vec{r}_2|$, they interpret the coefficient $D(\vec{r}_1)$ of s^2 as a measure of the delocalization of electrons at $\vec{r}_1$. The electron localization function

$$l(r) = [1 + (D(r)/D_0(r))^2]^{-1}, \quad (1)$$

which varies between 0 and 1, is thus taken to be a measure of localization. Here $D_0(r)$ is the value of $D(r)$ for free elec-

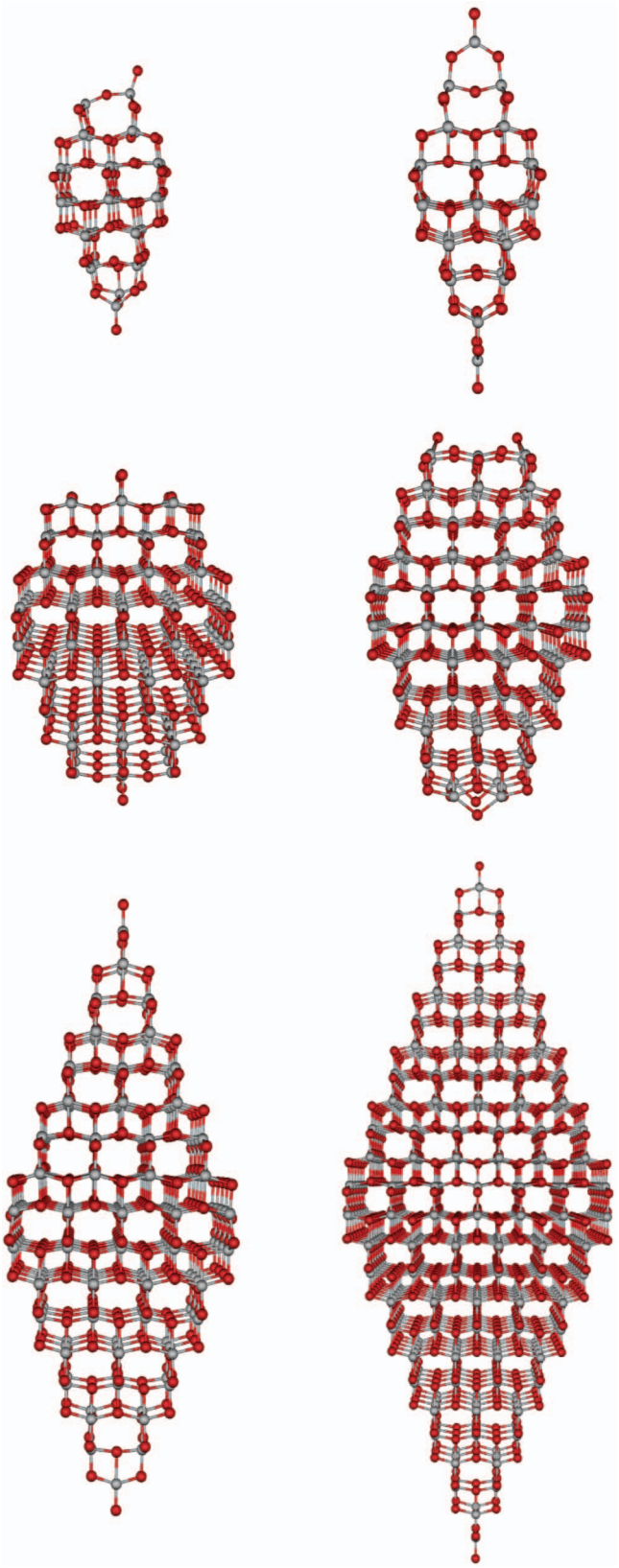

FIG. 4. (Color) SCTB relaxed structures of 99, 105, 417, 453, 495, and 1365 atom nanoparticles.

trons. A perfect localization corresponds to $l(r)=1$. The $D(r)$ is orbital independent, and can be defined solely in terms of the electron density $\rho(r)$. In closed shell systems, the ELF is very useful in determining the location of localized electrons, especially on surfaces.

Figure 2(b) shows a two-dimensional profile of the ELF though the central plane of the relaxed anatase nanoparticle containing the apex O atoms. The regions of high $l(r)\approx 1$ are colored red and low $l(r)\approx 0$ are colored blue, so that the color indicates the probability of localized electrons.

By applying an iso-surface to the ELF, a three-dimensional view can be generated (see Fig. 3). At a value of $l(r)=0.2$ and at a value of $l(r)=0.5$ (center of Fig. 3), little can be discerned (left of Fig. 3). However, at a value $l(r)=0.8$ (right of Fig. 3) the probable positions of localized electrons become more apparent. At a value of $l(r)=0.8$ the mushroom-cap iso-surfaces indicate a high probability of electrons being localized at the nanoparticle edges and vertices, but not at the center of the facets.

V. TIGHT BINDING RESULTS

A. Comparison of SCTB and first principles results for the 105 atom nanoparticle

Here we compare energies, geometries and electronic properties of the 105 atom nanoparticle calculated by the DFT and SCTB methods. From the SCTB calculation on the relaxed 105 nanoparticle, we find an excess energy ΔE per TiO_2 unit of 1.41 eV compared to 1.03 eV in the DFT calculation, see Table II. This difference probably arises because the SCTB model was fitted to results of bulk DFT calculations using the LDA, whereas the first principles results reported here used the DFT GGA with the PW91 functional. As reported in Table I the SCTB surface energy for a (101) anatase surface is somewhat below the LDA result but is higher than that found in the DFT GGA calculations. Since these surface energies probably dominate ΔE, we believe this difference is the main origin of the discrepancy.

In the SCTB calculation the apex-to-apex length of the relaxed 105 atom nanoparticle is 24.86 Å, whereas the first principles result was 22.82 Å. The relaxed bipyramidal side length was found to be 7.53 Å, whereas the first principles result was 7.47 Å. The bond length for the undercoordinated oxygen at the apex in the SCTB calculations contracts relative to the bulk Ti-O bond length to 1.85 Å.

To further compare the structures from the SCTB (Fig. 4) and DFT calculations we calculated radial distribution functions for both structures. The radial distribution functions are given in Fig. 5(a) for 105 atom nanoparticle. In both the DFT-optimized and the SCTB calculations, we find contraction of the Ti-O bonds, relative to bulk values, throughout the nanoparticle. In both the DFT-optimized and the SCTB calculations, we find contraction of the Ti-O bonds, relative to bulk values, throughout the nanoparticle. The $G(r)$'s for the DFT and SCTB 105 atom structures show good agreement in the peak positions corresponding to the first and next nearest neighbors, and also in the shoulder after the first peak. Slight differences in optimized lattice constants for two

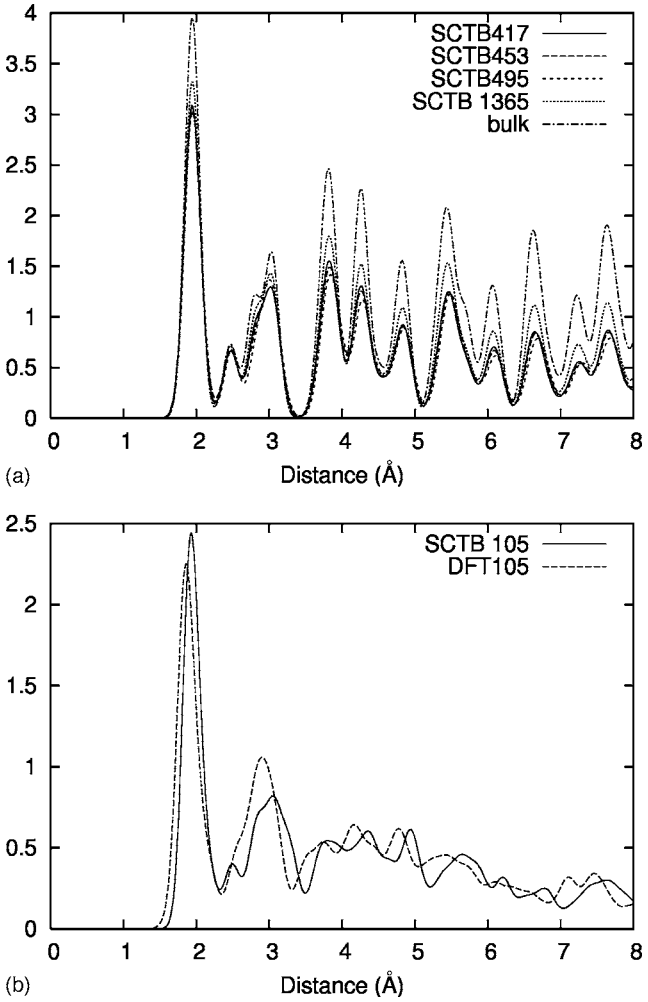

FIG. 5. Radial distribution functions for (a) relaxed SCTB structure of 105 atom nanoparticle and relaxed DFT structure of 105 atom nanoparticle, (b) relaxed SCTB structures of 417, 453, 495, and 1365 atom nanoparticles and bulk anatase. The radial distribution functions were obtained by Gaussian broadening (standard deviation $\sigma=0.1$ Å) of discrete interatomic distance distributions with the appropriate normalization factors.

methods and in the apex double bond length are observed in this figure.

The charge distribution of the SCTB method is illustrated in Fig. 6, where excess charge on the nanoparticle atoms relative to bulk atoms is presented for 105 nanoparticle. For the 105 atom nanoparticle, the largest changes, relative to bulk, are observed on the apex oxygens, where the ionicity is reduced due to formation of a stronger covalent bond and the charge is more positive relative to the bulk. The other significant change is for the central atom, which is surprising since it is the most bulk-like Ti atom. It is charged positively relative to the bulk Ti, i.e., becomes more ionic. Interestingly, the ECD distribution from our DFT results (see Fig. 2) does not show this electron depletion either due to the ECD resolution or the absence of the feature.

B. SCTB calculations on other nanoparticles

One of the advantages of the SCTB method is that the calculations are roughly two orders of magnitude faster than

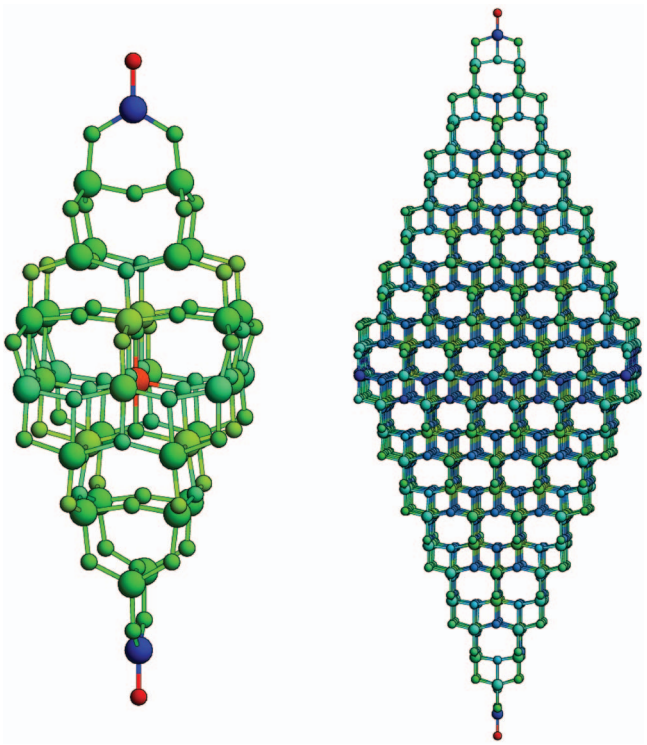

FIG. 6. (Color) Excess charge relative to bulk for 105 (left) and 1365 (right) atom nanoparticles from SCTB calculations. Red is more positive charge and blue is more negative charge.

the first principles ones. Therefore, the SCTB method was used to study the systematic changes in the properties of a series of anatase nanoparticles containing 99, 105, 417, 453, 495 and 1365 atoms. The 105, 495, and 1365 structures form a set of tetragonal bipyramids of increasing size bounded by {101} surfaces. The coordination of surface atoms is at least four for Ti and at least two for O with the exception of two apex oxygens for each nanocrystal having a double bond to a single threefold-coordinated Ti neighbor. These structures are stoichiometric, have a relatively high symmetry (D2d), preserve charge neutrality and have well defined facets. The last feature distinguishes our structures from the ones studied by Persson, Gebhardt, and Lunell.[29] Their study addressed electronic properties in which small stoichiometric anatase clusters form $Ti_{16}O_{32}$ to $Ti_{38}O_{76}$ with no particular surface orientation. The remaining structures (99, 417, and 453) are obtained by truncating the bipyramids in the (001) planes. Their consideration was motivated by the Wulff construction for macroscopic crystals that has {001} facets at the apices of an anatase crystal, yielding a truncated bipyramid. We did not find any atomic arrangements in the range up to 1500 atoms, which were stoichiometric and had ideal {100} and {101} facets as predicted by the Wulff construction in the limit of large crystals. However, these structures with 99, 417 and 453 atoms were stoichiometric and approximated the predicted Wulff ratio of {101} to {001} surface area, although we were forced to add or subtract a few atoms which rendered the {001} surfaces imperfect in order to preserve stoichiometry. The relaxed structures are shown in Fig. 4. All the relaxed cluster dimensions and excess energies calculated for this series of clusters calculated with SCTB, together with the first principles results for the 105 atom nanoparticle, are summarized in Table II. The excess energies become lower with increase in the nanoparticle size, decreasing from 1.41 eV per TiO_2 unit for the 105 atom particle to 0.56 eV for the 1365 atom particle. The structures proved to be stable and to have energies that scale smoothly as a function of crystal size for both bipyramidal and truncated bipyramidal structures.

The apex-to-apex length in the relaxed structures is 24.86 Å in the 105 atom nanoparticle, 42.19 Å in the 495 atom nanoparticle and 60.93 Å in the 1365 atom nanoparticle. The side length in all three nanoparticles (105, 495, and 1365) changes very little, less than 0.05 Å in SCTB optimizations. The bonds for undercoordinated oxygen at the apex shorten to 1.85 Å. Most structures are contracting with respect to the unrelaxed structure based on SCTB optimized bulk, much in the same way as occurred for the DFT structure of the 105 nanoparticle. We have verified that the relaxation does not significantly affect the D2d point symmetry of the initial tetragonal bipyramid (105, 495, and 1365) structures. Indeed, a fit of the optimized geometries to D2d produced uncertainties of 0.2% for the DFT 105 structure, 1.0% for the 105 SCTB structure, 0.3% for the 495 SCTB structure and 0.1% for the 1365 SCTB structure. The positions of peaks in $G(r)$ for the larger structures are very close to the bulk $G(r)$ since the bulk-like atoms dominate the structure [Fig. 5(b)]. The height difference of the peaks for these structures is due to finite spatial extent of the nanoparticles. Also, the peaks are slightly broader than for the bulk structure. Previous studies[29] of relaxation in $Ti_{16}O_{32}$ nanocrystal showed preservation of crystalline order in agreement with our observations.

The displacement of electronic charge from the center of the nanoparticle to the surface which was found in the 105 atom nanoparticle is not as pronounced in the larger particles as evident from the charge distribution for the 1365 atom nanoparticle in Fig. 6. The positive charge in larger nanoparticles is redistributed to a larger number of bulk-like Ti atoms. In comparison to the 105 atom nanoparticle, the apex oxygens of larger nanoparticles have reduced ionicity.

VI. CONCLUSIONS

DFT and self-consistent tight-binding calculations were performed for a bipyramidal 105 atom anatase nanoparticle. Full geometry optimization resulted in both surface relaxation and a slight overall contraction of the nanoparticle. Analyzing electronic properties using electron localization function and Mulliken populations, we found nonbonding electrons at the edges and corners of the nanoparticle. The results of tight-binding and DFT calculations are in reasonable agreement, suggesting the tight-binding scheme to be a useful tool for studies of larger nanoparticles in the range of hundreds to thousands of atoms. To explore the possibilities, we reported SCTB calculational results on five other nanoparticle structures containing 99, 417, 453, 495, and 1365 atoms. Some of these nanoparticles were bipyramidal and some were truncated bipyramids with imperfect (001) facets

TABLE III. Tight-binding parameters.

Parameter	a_4	a_5	a_6	a_7	a_8	a_9	a_{10}	a_{11}	a_{12}	a_{13}	R_0
Ti-O $t_{ss\sigma}$	−0.06458	−0.01491	−0.001029	−0.02359	−0.02653	0.03029	0.02420	0.04807	0.03944	0.04277	2.16
Ti-O $s_{ss\sigma}$	−0.02039	−0.02126	−0.002869	−0.001772	−0.005712	−0.003296	0.000187	−0.001133	0.002269	0.000860	2.16
Ti-O $t_{sp\sigma}$	0.02773	0.04525	0.04115	−0.01329	−0.03462	0.004176	−0.023200	−0.04838	−0.02446	−0.02557	2.08
Ti-O $s_{sp\sigma}$	0.015750	0.01230	0.01289	0.008079	0.007273	0.008502	0.000589	−0.000159	0.005211	−0.001447	2.08
Ti-O $t_{ps\sigma}$	−0.02899	−0.07721	−0.04243	0.01601	−0.05543	−0.01464	0.02232	0.004207	0.01071	−0.007085	2.07
Ti-O $s_{ps\sigma}$	−0.002296	0.000259	−0.006480	0.000919	0.001076	−0.002256	−0.004250	−0.003120	−0.005450	0.003488	2.07
Ti-O $t_{pp\sigma}$	−0.009599	0.03142	0.025260	−0.03673	0.03559	0.02176	0.04097	0.01781	−0.001847	0.02018	2.0146
Ti-O $s_{pp\sigma}$	−0.01465	−0.01535	−0.01281	−0.008943	−0.01068	−0.01132	−0.005736	−0.007696	−0.002742	−0.003422	2.0146
Ti-O $t_{pp\pi}$	0.04609	0.03701	0.07199	0.04340	0.04073	0.01072	0.05820	0.01094	−0.004518	−0.04674	2.0146
Ti-O $s_{pp\pi}$	0.01349	0.004183	0.01273	0.002277	0.008983	−0.000113	0.002415	−0.009627	−0.003925	0.000699	2.0146
Ti-O $t_{ds\sigma}$	−0.87721	10.24978	−11.79401	−26.13549	6.75205	47.13466	−26.97529	0.036907	0.04087	0.04397	2.1155
Ti-O $s_{ds\sigma}$	−0.23480	0.47223	0.34613	−0.14553	−0.45309	−0.37406	0.40653	−0.006157	−0.001788	−0.002064	2.11549
Ti-O $t_{dp\sigma}$	6.81294	−37.93371	27.78530	26.00079	−13.64912	−27.52159	16.16462	0.02644	0.01604	0.02888	1.94
Ti-O $s_{ps\sigma}$	−0.58135	4.06832	−3.92033	−3.05817	2.26911	3.63892	−2.35088	0.001335	0.000752	0.003254	1.94
Ti-O $t_{dp\pi}$	−3.07094	17.14109	−12.25218	−11.88011	5.35735	13.38596	−7.61512	−0.02506	−0.01348	−0.02028	1.93
Ti-O $s_{dp\pi}$	0.16224	−1.12603	1.12148	0.76906	−0.52675	−1.04910	0.65568	−0.001182	−0.000341	−0.002692	1.94
O-O $t_{ss\sigma}$	0.0	−1.10014	4.73575	−6.40288	2.52953	0.0	0.0	0.0	0.0	0.0	2.50
O-O $s_{ss\sigma}$	0.0	0.05171	−0.22356	0.30137	−0.11698	0.0	0.0	0.0	0.0	0.0	2.5
O-O $t_{sp\sigma}$	0.0	2.12781	−8.38372	10.47465	−3.88477	0.0	0.0	0.0	0.0	0.0	2.50
O-O $s_{sp\sigma}$	0.0	0.07978	−0.14405	−0.03658	0.06990	0.0	0.0	0.0	0.0	0.0	2.50
O-O $t_{pp\sigma}$	−3.46564	9.77548	−0.93872	−7.56622	−1.36908	6.59966	−2.29029	0.0	0.0	0.0	2.5
O-O $s_{pp\sigma}$	0.0	0.02926	0.03328	−0.22632	0.13159	0.0	0.0	0.0	0.0	0.0	2.50
O-O $t_{pp\pi}$	0.0	−0.41436	1.68449	−2.16722	0.82062	0.0	0.0	0.0	0.0	0.0	2.50
O-O $s_{pp\pi}$	0.0	−0.01099	0.02347	−0.002940	−0.005215	0.0	0.0	0.0	0.0	0.0	2.50
Ti-O E_s^{env}	0.20307	0.18763	0.19953	0.17939	0.15170	0.11048	0.07681	0.11878	0.01975	0.008908	1.95
Ti-O E_p^{env}	0.14696	0.19857	0.17254	0.23574	0.02169	0.06199	0.00605	0.001793	0.20194	0.04759	1.95
Ti-O E_d^{env}	−0.007124	0.003792	−0.06207	−0.01389	−0.06388	−0.05943	−0.04574	0.000829	0.20441	0.004065	1.95
O-Ti E_s^{env}	0.000181	0.124809	−0.03202	0.43394	0.22198	−0.58432	0.18006	0.007369	0.003261	0.005359	1.95
O-Ti E_p^{env}	0.007231	0.13552	−0.03835	0.50515	0.22406	−0.50711	0.16848	−0.01122	0.003875	0.004816	1.95
O-O E_s^{env}	0.0	0.0	−0.15181	0.23535	−0.17750	−0.10536	0.31289	0.0	0.0	0.0	1.95
O-O E_p^{env}	0.0	0.0	−0.15181	0.23535	−0.17750	−0.10536	0.31289	0.0	0.0	0.0	1.95

truncating the two apices of the pyramids. It is remarkable that the results for bipyramids and truncated bipyramids scale with the total number of atoms in almost the same way. We will explore different shapes of nanocrystals, as well as SCTB simulations of nanocrystals in water, in the future.

ACKNOWLEDGMENTS

This work has been supported by the U.S. Department of Energy, BES-Chemical Sciences, under Contract No. W-31-109-ENG-38, and BES-Materials Science, under Contract No. DE FG02-91-ER45455. Computational resources for this project have been supplied by Argonne National Laboratory—Laboratory Computing Resource Center, Minnesota Supercomputing Institute, Pacific Northwest National Laboratory Molecular Science Computing Facility and the U.S. Department of Energy National Energy Research Scientific Computing Center. The authors are grateful to M. Sternberg for useful discussions.

APPENDIX

The self-consistent tight-binding model we use to calculate the electronic structure and atomic forces at each stage of relaxation, is described in Refs. 18 and 19. The total energy expression of the system is given by

$$E_{\mathrm{tot}} = \sum_i E_i(Q_i,R) + \sum_{i,\mu,j,\nu} Q_{i\mu,j\nu}[\delta_{ij} v^{(1)}_{i\mu,j\nu} + (1-\delta_{ij}) t_{i\mu,j\nu}] + \frac{1}{2}\sum_{i\neq j} \frac{e^2(Z_i - Q_i)(Z_j - Q_j)}{R_{ij}}. \quad \text{(A1)}$$

Latin lower case subscripts $i,j,k,\ldots$ denote ionic sites and Greek lower case subscripts $\mu,\nu,\ldots$ denote orbitals $s,p,d,\ldots$.

Here, we define the charge Q_i in a nonorthogonal basis as

$$Q_i = \frac{1}{2}\sum_{\lambda} n_\lambda \sum_{\mu,j,\nu} c^*_{i\mu,\lambda} S_{i\mu,j\nu} c_{j\nu,\lambda} + c^*_{j\nu,\lambda} S_{j\nu,i\mu} c_{j\mu,\lambda}. \quad \text{(A2)}$$

$S_{j\nu,i\mu}$ is the overlap integral between the two orbitals $j\nu$, $i\mu$. Q_i can be interpreted as number of electrons at site i. The one body density matrix $Q_{i\mu,j\nu}$ is defined as $Q_{i\mu,j\nu} = \Sigma_\lambda n_\lambda c^*_{i\mu,\lambda} c_{j\nu,\lambda}$. We take $n_\lambda = 1$ for the lowest N values of ϵ_λ where N is the number of electrons and ϵ_λ is an eigenvalue of the effective one electron equation obtained from 2 by minimization with respect to the $c^*_{j\nu,\lambda}$. The $c_{j\nu,\lambda}$ describe the eigenvectors of this effective one electron equation. The terms $t_{i\mu,j\nu}$ are matrix elements of the kinetic energy and $v^{(1)}_{i\mu,i\mu}$ are electrostatic energy terms matrix elements containing multipole moments of the ions obtained from the multipole expansion of the Hartree term.[19] In the parametrization, the on-site energy $E_i(Q_i,R)$ contains two parts: The first describing the ions at infinite spatial separation is parametrized by the ionization energies of the ions as a function of their charge, and implicitly includes on-site exchange and correlation effects. The second part of $E_i(Q_i,R)$ depends on the positions of the neighbors of the ion i and takes account of core-core repulsion effects: $E_i = \Sigma_s \epsilon_s Q_{i,s} + \Sigma_l A_l Q_i^l + E_i^{env}$, where ϵ_s is the energy of one-electron Hartree-Fock orbital of the neutral atom in shell s. We take $\epsilon_s = 0$, $\epsilon_p = 3$ eV and $\epsilon_d = 0$ for titanium. The second term in E_i is fit to the ionic ionization potentials and electron affinities.[19] The last term in on-site energy has the $E_i^{env} = \Sigma_{i,j} Q_i u(R_{ij})$, where the interaction $u(R_{ij}) = \Sigma_{n=4}^{13} a_n (R^0_{ij}/R_{ij})^n$. In the present calculation for Ti, this is evaluated only for nearest-neighbor titanium-titanium pairs. $R^0_{ij} = 1.95$ A. The kinetic energy and overlap integrals $t_{i\mu,j\nu}$ and $S_{j\nu,i\mu}$ are parametrized by the same polynomial form in the inverse of the distance between the two ions in question that is used for $u(R_{ij})$ (but with different coefficients, of course). The parametrization of the multipole terms $v^{(1)}_{i\mu,i\mu}$ is described in reference Ref. 19. The parameters determining E_i^{env}, $t_{i\mu,j\nu}$, and $S_{j\nu,i\mu}$ are determined by fitting the results of the tight-binding model to the results of a data base of first principles results on the cohesive energy and band structures for a variety of atomic distortions of a periodically repeated unit cell of the bulk metal as described in the text. The resulting parameters are summarized in Tables III and IV where the matrix elements are described in the standard Slater notation in which the orbitals are referred to a local basis determined by the direction of the vector between the ions.[30]

TABLE IV. Tight-binding parameters.

Parameter	Value
$\langle s\|z\|p_z\rangle$	0.9 Å
$\langle s\|z\|p_z\rangle$	0.215 Å
$\langle p_z\|3z^2-r^2\|p_z\rangle$	−0.037467 Å^2
$\langle d_{3z^2-r^2}\|3z^2-r^2\|d_{3z^2-r^2}\rangle$	−0.10333 Å^2
$\langle d_{3z^2-r^2}\|35z^4-30z^2r^2+3r^4\|d_{3z^2-r^2}\rangle$	−0.3 Å^4

*Corresponding author. Electronic address: zapol@anl.gov

[1] W. F. Zhang, M. S. Zhang, Z. Yin, and Q. Chen, Appl. Phys. B: Lasers Opt. **70**, 261 (2000).
[2] T. Paunesku, T. Rajh, G. Wiederrecht, J. Maser, S. Vogt, N. Stojićević, M. Protić, B. Lai, J. Oryhon, M. Thurnauer, and G. Woloschak, Nat. Mater. **2**, 343 (2003).
[3] U. Diebold, Surf. Sci. Rep. **48**, 53 (2003).
[4] P. K. Naicker, P. T. Cummings, H. Zhang, and J. F. Banfield, J. Phys. Chem. B **109**, 15243 (2005).
[5] A. S. Barnard and P. Zapol, J. Chem. Phys. **121**, 4276 (2004).
[6] A. S. Barnard and P. Zapol, J. Phys. Chem. B **108**, 18435 (2004).
[7] H. Zhang and J. F. Banfield, J. Mater. Chem. **8**, 2073 (1998).
[8] H. Zhang and J. F. Banfield, J. Phys. Chem. B **104**, 3491 (2000).
[9] J. P. Perdew and Y. Wang, Phys. Rev. B **45**, 13244 (1992).
[10] G. Kresse and J. Hafner, Phys. Rev. B **47**, R558 (1993).
[11] G. Kresse and J. Furthmüller, Phys. Rev. B **54**, 11169 (1996).
[12] G. Kresse and J. Furthmüller, Comput. Mater. Sci. **6**, 15 (1996).
[13] D. M. Wood and A. Zunger, J. Phys. A **18**, 1343 (1985).
[14] D. Vanderbilt, Phys. Rev. B **41**, 7892 (1990).
[15] G. Kresse and J. Hafner, J. Phys.: Condens. Matter **6**, 8245 (1994).
[16] P. E. Blöchl, Phys. Rev. B **50**, 17953 (1994).
[17] G. Kresse and D. Joubert, Phys. Rev. B **59**, 1758 (1999).
[18] N. Yu and J. W. Halley, Phys. Rev. B **51**, 4768 (1995).
[19] P. K. Schelling, N. Yu, and J. W. Halley, Phys. Rev. B **58**, 1279 (1998).
[20] S. Erdin, Y. Lin, and J. W. Halley, Phys. Rev. B **72**, 035405 (2005).
[21] W. Kohn and L. J. Sham, Phys. Rev. **140**, A1133 (1965).
[22] N. Troullier and J. L. Martins, Phys. Rev. B **43**, 1993 (1991).
[23] Y. Lin, L. A. Curtiss, P. Redfern, J. Rustad, and J. W. Halley (unpublished).
[24] G. Wulff, Z. Kristallogr. Mineral. **34**, 449 (1901).
[25] S. P. Russo, A. S. Barnard, and I. K. Snook, Surf. Rev. Lett. **10**, 233 (2003).
[26] J. K. Burdett, T. Hughbanks, G. J. Miller, J. W. Richardson, Jr., and J. V. Smith, J. Am. Chem. Soc. **109**, 3639 (1987).
[27] A. S. Barnard and P. Zapol, Phys. Rev. B **70**, 235403 (2004).
[28] A. D. Becke and K. E. Edgecombe, J. Chem. Phys. **92**, 5397 (1990).
[29] P. Persson, J. C. M. Gebhardt, and S. Lunell, J. Phys. Chem. B **107**, 3336 (2003).
[30] J. C. Slater and G. F. Koster, Phys. Rev. **94**, 1498 (1954).
[31] M. Lazzeri, A. Vittadini, and A. Selloni, Phys. Rev. B **63**, 155409 (2001); **65**, 119901(E) (2002).